Biotemplated Silica and Silicon Materials as Building Blocks for Micro- to Nanostructures

Biotemplated Silica and Silicon Materials as Building Blocks for Micro- to Nanostructures

Noémie-Manuelle Dorval Courchesne,[⊥§] Stephen A. Steiner III,[‡§] Victor J. Cantú,[‡§] Paula T. Hammond,*[⊥§] Angela M. Belcher,*[‡§]

[⊥] Department of Chemical Engineering, Massachusetts Institute of Technology, 77 Massachusetts Avenue, Cambridge, MA, 02139, USA

[‡] Department of Materials Science and Engineering and Department of Biological Engineering, Massachusetts Institute of Technology, 77 Massachusetts Avenue, Cambridge, MA, 02139, USA

[§] The David H. Koch Institute for Integrative Cancer Research, 500 Main Street, Cambridge, MA, 02139, USA

ABSTRACT: Silicon is essential in several energy-related devices, including solar cells, batteries and some electrochemical systems. These devices often rely on micro- or nanostructures to function efficiently, and require patterning of metallic surfaces. Currently, constructing silicon features at the micro- and nanoscale requires top-down energy-intensive processes, such as e-beam lithography, chemical etching or anodization. While it is difficult to form silicon in aqueous solution, its oxide, silica, can easily be synthesized using sol-gel chemistry and nucleated onto templates with diverse shapes to create porous or continuous architectures. Here, we demonstrate that novel silica nanostructures can be synthesized via biomineralization, and that they can be reduced to silicon using magnesiothermal reduction. We selected three biotemplates to create silica structures with various aspect ratios and length scales. First, we use diatomaceous earth as a model silica material to optimize our process, and we also biomineralize silica onto two microorganisms, the high aspect ratio M13 bacteriophage, and the helical *Spirulina major* algae. During our process, the shape of the materials is preserved, resulting in silicon nanowires, nano-porous networks, spirals and other micro- and nano-structures with high surface area. Our method provides an alternative for the creation of silicon nanostructures, using pre-formed silica synthesized in solution. The process could be extended to a broader range of microorganisms and metal oxides for the rational design of on-demand micro- and nanostructured metals. In addition, we show that the intrinsic composition of the biotemplates as well as their growth medium can introduce impurities that could potentially be used as dopants in the final silicon structures, and that could allow for tuning the composition of n-doped or p-doped biotemplated silicon for use as semiconducting building blocks.

INTRODUCTION

Metalloid silicon is of paramount importance for several industrial applications, including the fabrication of semiconductors, solar panels and high strength alloys. In addition to using bulk silicon, there has been a growing interest in creating micro- and nanostructured silicon materials for applications in hybrid silicon-organic photovoltaics,[1] lithium-ion batteries,[2-3] micro-electronics,[4] and even sensing devices.[5-6] Organizing silicon into continuous structures can be used to improve charge transport, and creating high surface area networks could contribute to its reactivity and efficiency as an anode material. Silicon has the highest known theoretical charge capacity as an anodic material in lithium ion batteries,[7-9] and therefore developing new methods for the synthesis of high surface area silicon materials with on-demand nanostructures is of great interest. In addition, silicon is widely used for photovoltaic applications, and nanostructured silicon thin films are currently being explored for use as antireflection coatings, and in hybrid silicon solar cells which are inexpensive, low-temperature alternatives to conventional silicon solar cells.[1, 10]

Currently, patterning silicon is often carried out via top-down approaches, which include lithography combined with harsh chemical etching techniques,[11-14] electron-beam lithography,[15-17] or anodization[18-19] of silicon wafers. While these methods have been widely employed to create structures with simple geometries like silicon posts, pillars or nanowires, complex shapes cannot be achieved with these top-down approaches. A few novel silicon structures, including nanocrystals,[20 21] nanorods[22] and nanowires,[23] were also synthesized in high boiling point organic solvents and supercriticals fluids, but it remains challenging to form silicon under ambient and mild conditions. The ability to template metalloid silicon onto pre-assembled scaffolds with a desired shape would open up new possibilities for this material in the field of nanotechnology.

While silicon, due to its highly negative reduction potential, cannot be reduced from precursors in aqueous solution,[24] silicon dioxide or silica, is a material that can easily be synthesized via sol-gel reactions. Silica nanoparticle gels can be formed in solution, and subsequently nucleated onto scaffolds and templates that take on a variety of shapes. Now, with magnesiothermal reduction (MGTR), a process that has been recently developed to reduce metal oxides into their metal counterparts while preserving their shape, we can envision converting silica structures into metalloid silicon. MGTR was first investigated in the 1970's and 80's to prepare metals like boron[25] and titanium.[26-27] It was first applied to biologically-derived silica in 2007,[28] and since then, interest in creating various silicon nanostructures via MGTR has grown.

MGTR is the vaporization of magnesium at relatively low temperature (650 to 750 °C), and the reduction of a metal oxide,

such as silica, upon contact with its vapor. While silica is reduced to silicon, the vaporized magnesium is oxidized to magnesium oxide. This process can be carried out at temperatures considerably lower than the melting point of silicon (1414 °C), which allow for preserving the shape of the silica structure that is being reduced, in contrast with carbothermal processes that require temperatures above 1700 °C and cannot be used to create nanostructures.[29-30] It therefore allows for the formation of a variety of silicon structures with a precise control over the porosity, three-dimensional structure and grain size by exploiting and controlling well-known silica chemistries. During the past decade, MGTR has been employed to produce nanoporous silicon using diatoms[31], mesoporous silica granules, [32], silica particles grown on inorganic templates,[33] and rice husks[34] as precursors.

In order to produce a broader variety of silica shapes, with more complex or finer structures, we turned our attention to biological templates. Viruses, bacteria, algae and other microorganisms have a plethora of shapes that could be of interest for technological applications. They often exhibit complex morphologies containing turns, coils, angles, and pores, and their size varies from tens of microns for algae to nanometers for viruses. In addition, they can be organized into three-dimensional hierarchical structures via bioconjugation techniques to create porous films or arrays.[35-36] Proteins found in microorganisms like diatoms[37] and sponges[38 39 40] can catalyze the formation of biotemplated silica. Silica can also be mineralized onto biotemplates with different shapes and length scales, and the silica structures can be reduced while preserving the shape of the template. Scheme 1 shows an overview of the biomineralization and magnesiothermal reduction process.

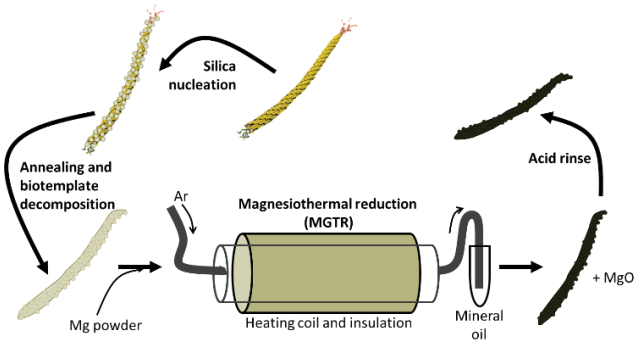

Scheme 1. Silica bio-mineralization and magnesiothermal reduction process. The process starts with a biotemplate onto which silica nanoparticles are nucleated. After annealing at high temperature to decompose the template and sinter the nanoparticles, the biotemplated silica is introduced into the magnesiothermal reactor along with Mg powder. The reactor is equipped with heating coils and insulation to reach the temperature required for magnesium vaporization and to maintain it. Argon is flowed in the reactor and any remaining magnesium vapors are collected in mineral oil at the outlet of the reactor. After the reaction, the silicon product is collected and impurities are removed with acid rinses.

The magnesiothermal reduction of silica proceeds as shown in Equation 1. Solid silicon powder is contacted with magnesium vapor, and is reduced to silicon.

$$SiO_{2(s)} + 2\ Mg_{(v)} \rightarrow Si_{(s)} + 2MgO_{(s)}\ (+\ Mg_2Si_{(s)}) \quad (1)$$

Magnesium oxide and magnesium silicide are formed as solid by-products, but can be easily rinsed off using an acid. For instance, with hydrochloric acid, magnesium oxide reacts to form magnesium chloride which is soluble in water (Equation 2), and magnesium silicide converts to micro-quantities of silane gas which bubbles out of solution (Equation 3). All purifications of the silicon products should be carried out in a fumehood to contain the toxic silane vapors and prevent exposure.

$$MgO_{(s)} + 2\ HCl_{(aq)} \rightarrow MgCl_{2(aq)} + H_2O \quad (2)$$

$$Mg_2Si_{(s)} + 4HCl_{(aq)} \rightarrow SiH_{4(g)} + 2\ MgCl_{2(aq)} \quad (3)$$

After rinsing off the by-products, the product is a pure silicon structure with the same shape as the biotemplate. The silicon product can be porous or continuous depending on the shape of the template and the silica mineralization conditions.

Of particular interest for the formation of silicon is diatomaceous earth (DE), a natural and abundant source of silica formed by the skeletal remains of diatoms. We used these natural fossilized silica structures as model low aspect ratio structures. In addition, many other microorganisms including viruses and algae can be used to nucleate silica nanoparticles. Here, the M13 bacteriophage, a filamentous bacteriophage, is used as a template to create silica nanowires. With its high aspect ratio – the phage has a length of 880 nm and diameter of 6.5 nm - the M13 bacteriophage is well known to generate fine nanowire-like structures upon biomineralization.[41 35] *Spirulina* major, a coil-shaped blue-green algae also serves as a template for silicon micro-coils. *Spirulina major* was recently used to mineralize titania[42] and copper[43 44] while preserving its spiral-like structure. We are therefore interested in demonstrating the use of this complex shape for the formation of silicon.

In this work we demonstrate our ability to bio-mineralize silica using the M13 bacteriophage and *Spirulina major* as templates, and to magnesiothermally reduce the products to silicon to form high surface area materials with defined nanostructures. Although the magnesiothermal reduction of DE has been previously demonstrated[28] and applied to battery anodes[45] and photoelectrodes,[46] we also use DE as a model organism to optimize the magnesiothermal reduction process. We then apply the optimal conditions to our biotemplated silica to produce novel silicon morphologies. We provide characterization of the morphology, elemental composition, and crystallinity of all biotemplated silica and silicon samples, and show that upon reduction, the as-synthesized amorphous silica is converted to nanocrystalline silicon and that the shape of the biotemplate is preserved throughout the process. In addition, we show that it is possible to first assemble the biotemplates into porous thin films, and then nucleate silica and reduce the thin films via magnesiothermal reduction to create porous silicon films with nanowire-like features. Interestingly, our results indicate that the novel coil and nanowire-like silicon morphologies that we present here could also act as semiconductors. We show that microorganisms have the potential for serving both as templates and sources of dopants for the production of semiconducting silicon. Our ability to produce high surface area and porous silicon materials could be extended to other metals and open up opportunities for using these materials to create aerogels, light weight structures and other useful porous metallic structures.

EXPERIMENTAL SECTION

Materials. Tetramethylorthosilicate (98%) (TMOS), silicon tetrachloride, ammonium hydroxide solution, dimethyl sulfoxide (DMSO), and magnesium powder were purchased from Sigma (St-Louis, MO). 3-isocyanatopropyltrimethoxysilane was purchased from Gelest (Morrisville, PA). Diatomaceous earth powder was purchased from DiatomaceousEarth.com (Lewisville, ID).

The E3 M13 bacteriophage variant was amplified by infecting exponentially growing Escherichia coli bacteria, and was separated and purified via centrifugation. DNA sequencing confirmed that the SFAAEEEDPAK peptide was displayed on each pVIII protein.

A starter culture of Spirulina major Alga-Gro® Seawater Medium were purchased from Carolina Biological Supply Company (Burlington, NC). 8 mL of Spirulina culture was added to 200 mL of growth medium in a sterile flask, and grown for at least 10 days without agitation, alternating between 12 hours in light and 12 hours in the dark.

Bacteriophage-templated silica nanoporous network synthesis. 100 µL of NH_4OH solution was added to 5.6 mL of DMSO and thoroughly mixed. On ice, $8e^{14}$ pfu of bacteriophage dissolved in 1.5 mL of water was added to the mixture. Ice was used to cool down the heat of mixing that was produced. The DMSO/NH_4OH/phage mixture was then added to 50 µL of TMOS in a separate vial, which was left at room temperature for 3 hours. The resulting entangled silica nanowires were precipitated by adding ethanol and toluene, and centrifuged down at 3000 rpm for 10 min. After further rinsing with ethanol, the silica nanowire pellet was dried in a vacuum oven at 80 °C overnight. To remove residual salts, the dried phage-templated silica was rinsed with milli-Q water, collected by centrifugation and dried again, twice. The bacteriophages were burnt off and the silica annealed in a tube furnace in air at 500 °C for 12 hours. Two more rinses with water, centrifugation and drying steps were performed to clean the nanoporous silica.

Porous bacteriophage-based silica thin film synthesis. Nanoporous bacteriophage thin films were assembled via covalent layer-by-layer, as described previously.[35] The films were rinsed with milli-Q water. A 0.2 M $SiCl_4$ solution was prepared by slowly pouring concentrated $SiCl_4$ on iced water, with agitation and allowing the ice to melt to form a solution. The bacteriophage films were immersed in this solution and incubated for 1 h at 80 °C. The silica-coated bacteriophage films were then rinsed with milli-Q water, blow-dried with nitrogen and annealed in air at 500 °C for 12 hours.

Spirulina-templated micro-coil synthesis. A section of Spirulina biofilm was taken directly from the growth flask and transferred into milli-Q water to rinse off minerals and salts. The rinsed film was deposited on a non-stick Teflon-lined surface and rinsed several times with acetonitrile. The film was then incubated on this surface for an hour in a 20 vol% 3-isocyanatopropyltrimethoxysilane solution in acetonitrile, and then rinsed with acetonitrile. An overnight incubation in a solution containing TMOS and ammonium hydroxide (NH_4OH) in DMSO followed, and the silica-coated biofilm was finally rinsed several times with DMSO and dried via lyophilization. To remove carbon and burn off the biotemplate, the silica-coated *Spirulina* film was exposed to oxygen plasma for 1 hour, and annealed at 500 °C for 12 hours in air in a tube furnace. Final rinses with milli-Q water and drying cycles were performed to clean the micro-coils.

Magnesiothermal reduction. A known mass of silica powder was placed in a stainless steel boat, along with magnesium powder in an adjacent boat (in general 10 mg of silica and 10 mg of magnesium), and pushed to the middle of a (1 in in diameter by 10 in in length) tubular reactor. Alternatively, a ~ 1 cm^2 thin film of silicon was placed in the reactor along with 2 mg magnesium. Argon was flowed through the reactor at a rate of 100 sccm, and the temperature was elevated to at least 600°C for 3 hours. After cooling down, the silicon product was removed from the reactor and residual MgO and Mg_2Si by-products were dissolved by immersing the sample in 1 M hydrochloric acid for 12 hours. The purified silicon product was thoroughly rinsed in milli-Q water, and dried in air.

Nanomaterial characterization. The morphology of the nanomaterials before and after magnesiothermal reduction was characterized using transmission electron microscopy (TEM) with a JEOL 2010 FEG Analytical Electron Microscope and scanning electron microscopy (SEM) with a Helios Nanolab 600 Dual Beam Focused Ion Beam Milling System. Spirulina-based materials were also observed by optical microscopy using a Leica LEITZ DMRX light microscope with a Nikon digital camera DXM1200F. The surface composition and chemistry of the samples was analyzed by X-ray photoelectron spectroscopy (XPS) with a PHI Versa-Probe II X-ray photoelectron spectrometer with a scanning monochromated Al source (1,486.6 eV; 50 W; spot size, 200 µm). X-ray diffraction (XRD) was used to evaluate the crystallinity of the samples, using a PANalytical Multipurpose Diffractometer and zero background holders. The surface area of the materials was measured by the Brunauer, Emmett and Teller (BET) technique, using an ASAP 2020 BET and monitoring nitrogen or krypton gas adsorption and desorption.

RESULTS AND DISCUSSION

DE was used as a model microorganism to demonstrate and optimize our magnesiothermal reduction process. The top panel of Figure 1 shows the morphology and color of DE before reduction. Using this abundant source of biotemplated silica, the reduction time and temperature were varied, as well as the mass of magnesium and the nature of the acid used for the post-reduction rinse (see Supporting Information, Figure S1, for XRD data). We established that the reduction must be carried out for 3 h in order to fully convert amorphous silica into crystalline silicon, and that the temperature should be kept at 650 °C or higher in order for the reaction to proceed. For a 10 mg silica sample, an equivalent mass of magnesium was found to be optimal for the reduction, which corresponds to a 2.5:1 Mg:SiO_2 molar ratio. A slight excess of magnesium is therefore desirable for the reaction to proceed. The by-products were easily removed by a rinse with a strong acid like HCl, while traces of MgO could still be detected by XRD after rinsing with a combination of two weak acids, acetic acid and formic acid. XPS also showed a complete removal of MgO after acid rinse (see Figure S2).

Under optimized conditions, reduced DE exhibit the morphology shown in the bottom panel of Figure 1. Before and after MGTR, it consists of a mixture of diatom shapes that are consistent with previous reports of reduced DE.[31] As indicated on the images, the size of the DE features decreased by almost two times. The diameter of cylindrical diatomaceous earth changed

from 15.2 ± 2.2 μm to 8.4 ± 2.2 μm. In addition, a drastic change in color occurred and indicated the presence of nano-sized silicon after reduction.

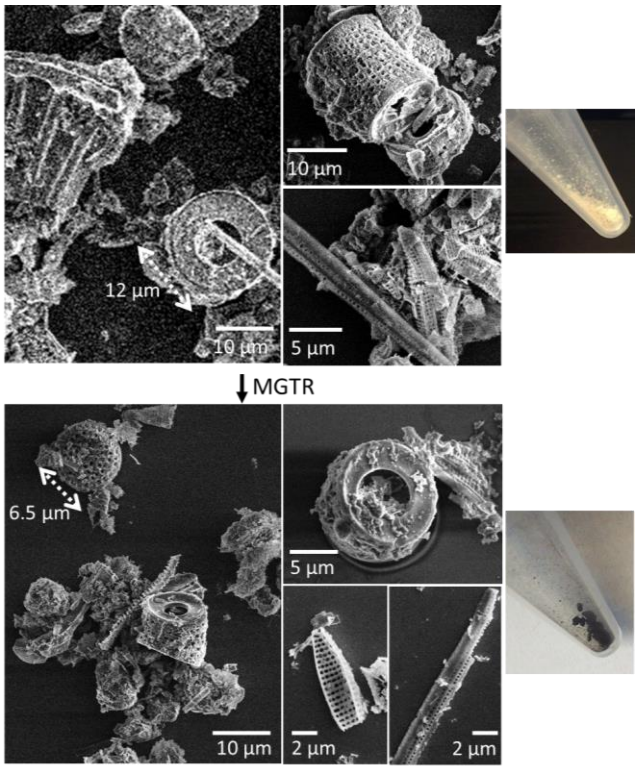

Figure 1. Upon magnesiothermal reduction, diatomaceous earth features shrink, but their shape is preserved. SEM and optical images of DE before (top) and after (bottom) reduction.

For a 3 h magnesiothermal reduction at 725 °C, the surface composition and crystallinity of DE were characterized, as shown in Figure 2. While only silica can be observed on the surface of the sample before reduction, silicon can be detected in the final product (XPS Si2p peak around 98.5 eV). Surface oxides are still present in the product due to normal oxidation of the surface during HCl rinse and under ambient atmosphere. If desired, these oxides could be removed via HF etching, but we did not perform this treatment in this work. XRD also indicates the presence of amorphous silica in DE before reduction, and shows peaks characteristic of nanocrystalline silicon after reduction. The additional peaks observed before reduction are attributed to salts and trace clay minerals that are also present in DE.[47]

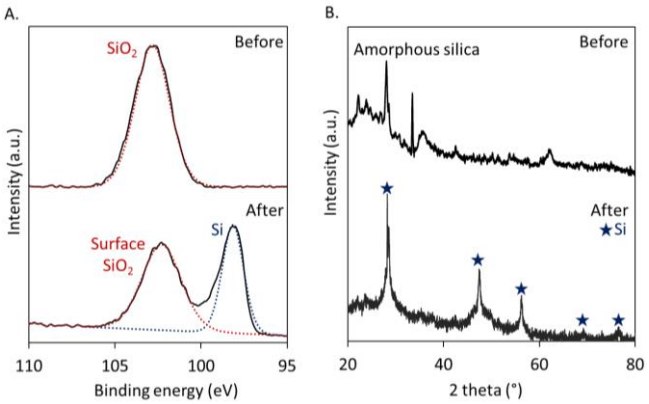

Figure 2. Magnesiothermal reduction converts amorphous diatomaceous earth silica to nanocrystalline silicon. XPS spectra showing the Si2p region (A) and XRD spectra (B) for DE before and after a 3 h reduction.

The magnesiothermal reduction process was then applied to biomineralized silica using M13 bacteriophage as a template. Silica nanoparticles were nucleated onto M13 bacteriophages in solution using TMOS as a precursor, and the reaction proceeded as shown in Equation 4. Dimethylsulfoxide (DMSO) was selected as a solvent in order to prevent denaturation of the bacteriophage template.

$$Si(OCH_3)_4 + 2\ H_2O \rightarrow SiO_2 + 4\ CH_3OH \quad (4)$$

The reaction time was optimized (see Supporting Information, Figure S3), and after a 3 h reaction, bacteriophage-templated nanoporous silica with a structure shown in Figure 3A (top) was synthesized. High aspect ratio features resembling entangled flexible and curved nanowires can be observed, with a nanowire diameter in the order of 10 to 15 nm and an average of 11.2 ± 1.8 nm. These nanowires form a porous network of silica. After drying the product, annealing the structure and burning off the bacteriophage template at 500 °C in air, a white powder was obtained. The bottom panel of Figure 3A shows the product after magnesiothermal reduction and acid rinse. This product exhibits a high porosity (~ 40 %, with pores generally smaller than 25 nm in diameter, see Supporting Information, Figure S4 for details) derived from the silica nanowire network, but its macroscopic color changed from white to dark brown/black, indicative of the conversion of silica to silicon.

Silica nanoparticles can also be nucleated onto a pre-assembled biotemplated network. For instance, M13 bacteriophages assembled into a porous thin film using a covalent layer-by-layer assembly process[35] can be fully infiltrated with silica nanoparticles using silicon tetrachloride as a precursor. By immersing the bacteriophage thin film in an aqueous $SiCl_4$ solution, the precursor hydrolyzes and silica nucleates specifically onto the thin film (Equation 5).

$$SiCl_4 + 2\ H_2O \rightarrow SiO_2 + 4\ HCl \quad (5)$$

Figure 3B (top) shows the structure of the resulting bacteriophage-templated silica film after burning off the bacteriophage template. When the template is removed, the silica nanoparticles nucleated along the phage sinter together to form filled fine nanowires. Similarly, this thin film was magnesiothermally reduced, and its final surface morphology is shown at the bottom of Figure 3B. A well-defined network of silicon nanowires is then created uniformly onto the substrate, which exhibits a dark color after reduction. The diameter of the nanowires is in average 11.5 ± 1.2 nm. The porosity of the silicon thin film approaches 30 %, and pores have diameters smaller than 40 nm with an average of 17 nm (see Supporting Information, Figure S4). This method provides a means to uniformly coat large surfaces with porous silicon. It also allows for the formation of considerably finer silicon features compared wtih those previously achieved to form mesoporous silicon via MGTR.[48 49]

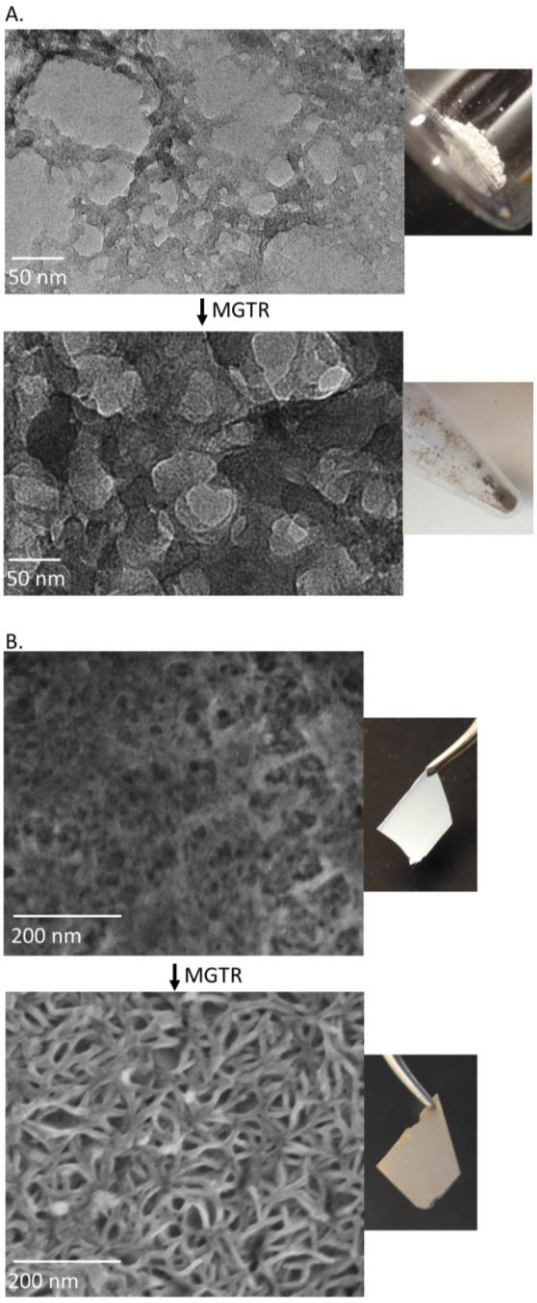

Figure 3. Silica and silicon interconnected nanoporous networks are produced with the M13 bacteriophage as a template. A. TEM and optical images of M13 bacteriophage-templated silica (top) and reduced silicon (bottom) nanowires synthesized in solution. B. SEM and optical images of silica (top) and reduced silicon (bottom) nanoporous networks templated by an LbL-assembled M13 bacteriophage thin film.

Bacteriophage-templated silica and silicon powders were characterized via XPS and XRD (Figure 4). XPS shows that the surface content of silica decreases upon reduction and that reduced species are also present (Si2p peak showing the presence of silicon and sub-oxides around 99.7 eV). From XRD measurements, it is determined that bacteriophage-templated silica was amorphous, and that it is converted to nanocrystalline silicon after magnesiothermal reduction.

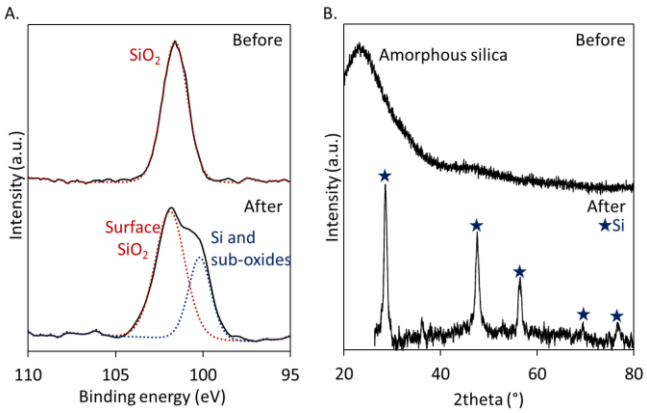

Figure 4. M13 bacteriophage-templated amorphous silica nanowires are converted to nanocrystalline porous networks of silicon. XPS spectra showing the Si2p region (A) and XRD spectra (B) for M13 bacteriophage-based silica and silicon nanowires synthesized in solution before and after reduction.

Spirulina major was used as a third biotemplate to produce silica and silicon structures. After at least 10 days of growth, the algae could be harvested as biofilms, and observed under optical microscope to reveal loose coil structures (see Figure 5A). The diameter of the *Spirulina* coils ranges between 2.5 and 3 μm, and a turn spans ~ 4.5 μm. Conveniently, *Spirulina* biofilms exhibit a mechanical resistance that allows them to stay intact when removed from the growth medium, and to maintain their shape even after silica nucleation. To nucleate silica on *Spirulina* biofilms, a silane with an isocyanate functional group was used to first nucleate silane molecules onto the polysaccharide layer that is known to surround each *Spirulina* algae (see Supporting information, Figure S5, for a TEM image showing *Spirulina* with its native polysaccharide layer). [50] This takes place because the hydroxyl groups that are present on the surface of *Spirulina* can react with the isocyanate functionalized silane molecules. Then, TMOS was used to synthesize a thicker layer of silica along the algae. Figure 5B shows a *Spirulina* biofilm lyophilized after silica biomineralization. Spiral-like entangled structures can be observed by SEM.

To remove the *Spirulina* template, the silica-coated biofilm was oxygen plasma treated for 1 h, and then annealed in air at 500 °C for 12 h. Figure 5C shows that the micro-coil shapes are preserved after burning off the template, and that individual spiral structures can be observed. After magnesiothermal reduction, similar silicon structures can be observed (see Figure 5D). Both for the *Spirulina*-templated silica and silicon, large entanglements of micro-coils are found and result directly from the structure of the *Spirulina* biofilm. Individual coils correspond to free algae that were mineralized with silica, or algae at the edge of the biofilms. The size of these individual hollow silicon structures is constant, with a diameter of 0.7 ± 0.1 μm. SEM with elemental mapping confirmed the presence of silicon co-localizing with the coils observed (see Supporting Information, Figure S6).

In addition to the change in color of the *Spirulina*-templated biofilms observed before and after reduction (see Figure 5C and 5D), XPS confirmed the presence of additional silicon chemistries after reduction, including a peak corresponding to metalloid silicon (around 99.5 eV). A single silica peak was measured before reduction, while fitting indicates that silicon is present in addition to surface oxides and sub-oxides in the sample after reduction (Figure 6A). As shown in Figure 6B, XRD also

confirmed the transformation of amorphous silica into bulk nanocrystalline silicon after reduction.

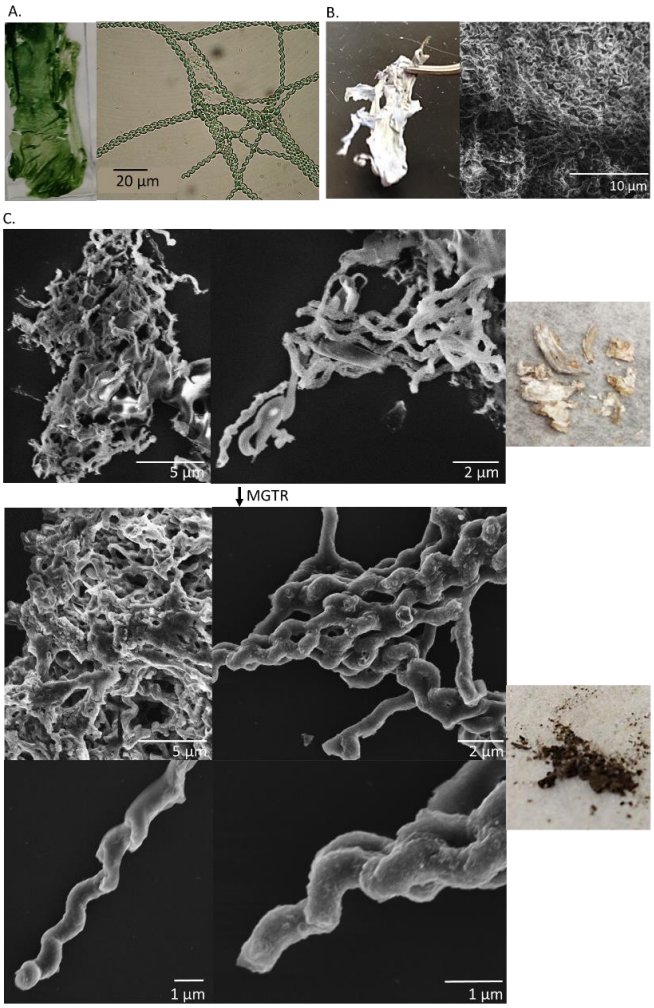

Figure 5. Silica and silicon micro-coils are formed using *Spirulina major* as a template. A. *Spirulina major* biofilm, as grown. B. Lyophilized silica-coated Spirulina biofilm. Optical image (left) and SEM image (right). C. Magnesiothermal reduction of *Spirulina*-templated silica. SEM and optical images of *Spirulina*-templated silica after annealing (top), and resulting *Spirulina*-templated silicon (bottom).

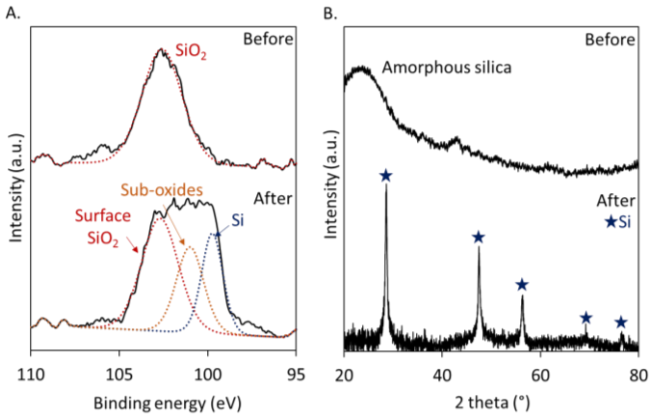

Figure 6. Spirulina-templated amorphous silica is converted to nanocrystalline silicon upon magnesiothermal reduction. XPS spectra showing the Si2p region (A) and XRD spectra (B) for *Spirulina*-templated silica and silicon micro-coils.

Quantifying the surface area of biotemplated silicon is of great importance for incorporating it in actual devices with specific design requirements and constraints. Large surface area materials are often desired to create large contact areas between two materials that may lead to increased reaction rates, or more efficient transport phenomena. On the other hand, a lower surface area might be desirable to reduce recombination rates in photoactive devices. We therefore assessed the surface area of our materials before and after magnesiothermal reduction. First, compared with a silicon nanoparticle control synthesized without biotemplate, the surface area of all biotemplated samples is lower (See Supporting Information, Figure S8). This difference results from the higher order organization of the nanoparticles along the biotemplates, to create high aspect ratio structures with reduced exposed surface area. Second, the data presented in Table 1 shows that, for all biotemplates, the surface area significantly increases upon reduction. This increase is due to the loss of oxygen atoms from the materials, as well as the change in crystallinity. M13 bacteriophage-templated nanoporous silicon exhibits the largest surface area of approximately 271 m^2/g. Conversely, *Spirulina*-templated silica and silicon have a smaller surface area compared to their diatom or bacteriophage-templated counterparts, which is consistent with the larger length scales of the *Spirulina* templates.

Table 1. BET Surface Area (m^2/g) of Biotemplated Materials Increases when Silica is Reduced to Silicon. Isotherms can be found in Supporting Information (Figure S7).

Biotemplate	Silica	Silicon
Diatomaceous earth	64	188
M13 bacteriophage	51	271
Spirulina major	19	43

We also estimated the silicon crystallite size in our biotemplated samples. This parameter can be of importance in terms of concentration of surface defects and interfaces within the material, and also for determining the properties of nanoscale silicon materials. The particle size of silicon in each of the samples was therefore calculated from their XRD spectra, using the Scherrer equation. Overall, the particle size ranges between ~10 and 25 nm, as shown in Table 2. Silicon templated using DE and the M13 bacteriophage have similar crystallite size, while silicon templated with *Spirulina major* has significantly larger particle size. This can be explained by the longer silica nucleation performed on the *Spirulina* templates. Because the features of *Spirulina major* are much larger than that of the M13 bacteriophage, a longer TMOS hydrolysis and condensation is necessary to fully cover the surface of the algae. Consequently, the silica and silicon particle size also increases since the reaction proceeds for longer. These results are also consistent with the lower surface area of *Spirulina*-templated silicon. In addition, smaller silica particles were expected to be nucleated onto the surface of M13 bacteriophages compared to *Spirulina major* because of the proximity of the nucleation sites on the coat proteins of the bacteriophages. Often, using M13 bacteriophages to nucleate materials tends to reduce the particle size.[51]

Table 2. The crystallite size for biotemplated silicon was calculated from XRD spectra using the Scherrer equation.

Biotemplate	Crystallite size (nm)
Diatomaceous earth	11.9 ± 2.9
M13 bacteriophage	13.3 ± 1.3
Spirulina major	23.9 ± 2.9

Although the conversion of silica to silicon is complete upon magnesiothermal reduction, other trace elements are found in the final biotemplated silicon materials, and their role needs to be understood in order to apply the materials to energy-relevant devices. In DE-based silicon, the main trace element found is aluminum, at an atomic concentration ranging between 0.2 and 1 % (Figure 7A left panel). The presence of Al is not surprising since DE is composed primarily of silica, but can also contain some clay minerals such as alumina. Upon magnesiothermal reduction, the alumina present in DE is reduced to Al, which could act as a p-type dopant in the final product. On the contrary, phosphorous is present in the final bacteriophage-templated nanoporous silicon, at an atomic concentration of 0.4 to 2 % (Figure 7A, middle panel). This P content likely originates from the DNA of the bacteriophage, and from the buffer solution chosen to suspend the bacteriophages. Nonetheless, the presence of P in silicon nanowires is promising for applications as n-type semiconductors. In *Spirulina*-templated silicon, magnesium is observed at an atomic concentration of ~ 0.3 % (Figure 7A, right panel). The presence of Mg is due to the chlorophyll pigment found in this algae, which contains an Mg center. Even after acid rinsing the magnesiothermally reduced *Spirulina*-templated silicon materials, Mg is still present, indicating that it must be trapped within the silicon structure. Such Mg-doped silicon spirals could be used as n-type semiconductors.[52]

In addition to phosphorous, a high sodium content was initially found in the bacteriophage-based nanowires if no water rinse was performed after synthesis. Water rinses at various steps of the process are necessary for fully removing sodium ions (See Supporting Information, Figure S9). Rinsing silicon templated onto LbL-assembled bacteriophage films also allows for tuning the concentration of phosphorous in the nanoporous silicon thin films from approximately 1 to 2.5 %, as shown in Figure 7B. If the bacteriophage films are taken directly after LbL assembly, they can contain as much as ~ 3 % phosphorous, due to the phosphate buffer used during LbL assembly. However, when the films are thoroughly rinsed with water after assembly, the phosphorous content is decreased to ~ 1%. Adding dopants, such as phosphoric acid during the silica mineralization, also allows for modifying the phosphorous content in the final silicon film.

The 1 % P content observed after rinsing the LbL films is consistent with the theoretical maximum amount of phosphorous that could dope silicon directly from the bacteriophage DNA. Considering the crystalline density of cubic crystals of silicon, one can determine that 8 Si atoms compose one unit cell, with a known cell volume of $(0.543\ nm)^3$.[53] This corresponds to a silicon atom density of $5e^{22}$ Si atoms/cm^3. Then, the volume of a bacteriophage-based silicon nanowire can be approximated as a cylinder of 880 nm in length, and the total number of silicon found in such a wire can be easily calculated. The phosphorous concentration deriving from the bacteriophage DNA is thus simply the ratio of the 7222 P atoms found in the 7222 bases that constitutes the single-stranded DNA genome of a bacteriophage,[54-55] over the number of silicon atoms in a phage-based silicon wire. Based on the geometry of the bacteriophage-based silicon nanowires, the phosphorous content due to DNA in a bacteriophage-templated silicon nanowire reaches 0.2 to 1 %. This percentage thus refers to the minimum phosphorous content in bacteriophage-templated silicon, and is equivalent to a dopant concentration of $1e^{21}$ to $5e^{21}$ P atoms/cm^3, resulting in heavily n-type doped materials.

Other trace elements could be introduced on-demand in the various biotemplated silicon materials by changing the microorganism growth and purification conditions, and the buffer solutions used at different stages of the process. Further experiments could lead to the production of useful biotemplated semiconductors and the precise quantification and tuning of the resulting n-type or p-type carrier concentrations.

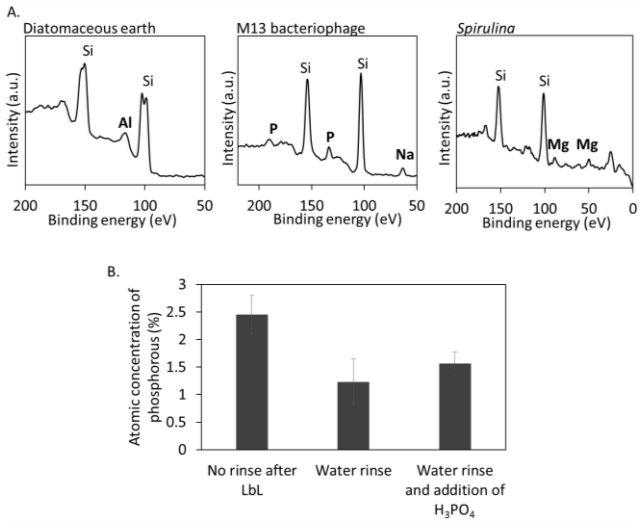

Figure 7. Intrinsic biotemplate composition and growth medium or buffer components contribute to doping the final silicon products. A. Sections of XPS survey scans showing the impurities in reduced biotemplated silicon. B. Phosphorous concentration in silicon templated onto LbL-assembled bacteriophage films, with or without rinses or phosphoric acid addition. The concentrations were averaged from at least three surface XPS measurements.

In addition to tuning the composition of the final biotemplated silicon products with impurities, the nature of the products can be modified by the process conditions. More specifically, carbides and nitrides can be synthesized instead of metals if biotemplated oxides are magnesiothermally reduced without burning off the organic template, or if the MGTR is carried out under a nitrogen environment, respectively. Scheme 2 summarizes the materials that can be synthesized by varying process conditions. For all the data presented in this work, the first process flow was followed; (1) the biotemplate was burnt off at high temperatures or using a combination of plasma treatment and high temperature annealing, (2) inert argon gas was flowed through the MGTR reactor, and (3) a metal or metalloid was obtained. If this process flow is modified by leaving the biotemplate in, the large amount of carbon present during the MGTR will cause the appearance of carbides. In the case of silica, the expected product will be silicon carbide. Alternatively, if the biotemplate is burnt off, but nitrogen is flowed through the reactor instead of argon, then nitrides can be

formed. After reducing silica, silicon nitride is the expected product.

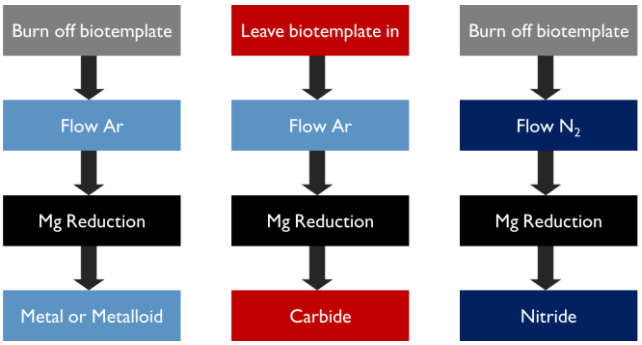

Scheme 2. Three different process routes lead to different products after magnesiothermal reduction: metals, carbides or nitrides.

For a reaction carried out under nitrogen and with silica still containing the bacteriophage template, we have observed the formation of silicon nitride and silicon carbide (see Supporting Information, Figure S10, for details). Silicon carbide and silicon nitride materials could also be applied to useful devices. For instance, porous silicon carbide could be of interest for the fabrication of temperature-resistant membranes due to the high thermal shock resistance of this material combined with its remarkable mechanical properties, or for use as a thermoelectric material due to its high thermal conductivity.[56-57] Silicon nitride also has attractive properties for a variety of applications. For example, it can act as an antireflective coating in photovoltaic devices,[58] and has also been studied for incorporation in waveguides.[59] Combining silicon nitride and silicon carbide materials has also attracted interest for taking advantage of the properties of both materials and improving mechanical and dielectric properties of the product.[60]

CONCLUSIONS

In conclusion, we have demonstrated that combining a biotemplated approach to nucleate silica nanoparticles along with magnesiothermal reduction represents a versatile process to create silicon nano- and microstructures. Complex shapes such as coils and entangled nanowires can be produced with this method. Individual microorganisms can serve as templates for discrete shapes, or they can be assembled into thin films to create three-dimensional networks. As-grown biofilms can even be used directly as templates, like the *Spirulina major* biofilm, or cross-linked microorganisms that can be synthetically drawn into higher order structures, like M13 bacteriophage porous thin films.

We have shown that amorphous silica is first nucleated onto the biotemplates via hydrolysis reactions, and that the template can be removed with heat treatments. After magnesiothermal reduction, the remaining silica is converted into nanocrystalline silicon, while preserving the original shape of the template. During the reduction process, the size of the features decreases, and as a consequence the specific surface area of the material increases. The process can therefore be used to synthesize high-surface-area biotemplated silicon building blocks.

In addition, our investigations of the elemental composition of the final silicon products reveal that biotemplates can serve as a sources of dopants to produce potentially semiconducting materials. Changing the reaction conditions would also allow for modifying the composition of the biotemplated silicon products.

While we have demonstrated this process with diatomaceous earth, the M13 bacteriophage, and *Spirulina major*, the concept could be extended to a broader range of microorganisms. Different oxide nanoparticles could also be synthesized on the biotemplates, and subsequently reduced to produce metallic structures with different compositions, including pure metals, doped semiconductors, and alloys.

ASSOCIATED CONTENT

Supporting Information. Process optimization data and additional characterization including: morphology of biotemplated silicon, BET surface area analysis, sodium removal via water rinses, and synthesis of silicon carbide and nitride. This material is available free of charge via the Internet at http://pubs.acs.org.

AUTHOR INFORMATION

Corresponding Author

* E-mail: Belcher@mit.edu, Hammond@mit.edu

Author Contributions

N.-M.D.C., S.A.S., P.T.H and A.M.B. conceived the idea and designed the experiments. N.-M.D.C., S.A.S. and V.J.C. performed the experiments and analyzed the data. The manuscript was written through contributions of all authors. All authors have given approval to the final version of the manuscript.

Funding Sources

Discretionary funds were used to support this research.

ACKNOWLEDGMENT

This work made use of the MIT MRSEC Shared Experimental Facilities supported by the National Science Foundation under award number DMR-0819762. The authors wish to express their appreciation to the Institute for Soldier Nanotechnologies at MIT, supported by the Army Research Office and Army Research Laboratories, whose facilities and equipment were used to conduct the research reported in this paper. N.-M.D.C. gratefully acknowledges support from an Eni-MIT Energy Fellowship through the MIT Energy Initiative Program, and from a Postgraduate Scholarship from the Natural Sciences and Engineering Research Council of Canada (NSERC)

ABBREVIATIONS

BET, Brunauer, Emmett and Teller; DE, Diatomaceous earth; SEM, Scanning electron microscopy; TEM, Transmission electron microscopy; TMOS, Tetramethylorthosilicate; XPS, X-ray photoelectron spectroscopy; XRD, X-ray diffraction.

REFERENCES

(1) T. Song, S.-T. Lee, B. Sun Silicon nanowires for photovoltaic applications: The progress and challenge, *Nano Energy* **2012**, *1*, 654-673.

(2) M. Ge, Y. Lu, P. Ercius, J. Rong, X. Fang, M. Mecklenburg, C. Zhou Large-Scale Fabrication, 3D Tomography, and Lithium-Ion Battery Application of Porous Silicon, *Nano Letters* **2014**, *14*, 261-268.

(3) T. Mokkelbost, E. Sheridan, A. Fossdal, A. M. Martinez, Ø. Dahl The Effect of Synthesis Routes for Preparation of Si Nanostructures for Lithium Ion Battery Anodes, *Meeting Abstracts* **2011**, *MA2011-01*, 586.

(4) Y. Yang, Y. Hwang, H. A. Cho, J.-H. Song, S.-J. Park, J. A. Rogers, H. C. Ko Arrays of Silicon

Micro/Nanostructures Formed in Suspended Configurations for Deterministic Assembly Using Flat and Roller-Type Stamps, *Small* **2011**, *7*, 484-491.
(5) F. A. Harraz Porous silicon chemical sensors and biosensors: A review, *Sensors and Actuators B: Chemical* **2014**, *202*, 897-912.
(6) P. Inkyu, L. Zhiyong, P. P. Albert, R. S. Williams Top-down fabricated silicon nanowire sensors for real-time chemical detection, *Nanotechnology* **2010**, *21*, 015501.
(7) U. Kasavajjula, C. Wang, A. J. Appleby Nano- and bulk-silicon-based insertion anodes for lithium-ion secondary cells, *Journal of Power Sources* **2007**, *163*, 1003-1039.
(8) Y. Zhang, X. G. Zhang, H. L. Zhang, Z. G. Zhao, F. Li, C. Liu, H. M. Cheng Composite anode material of silicon/graphite/carbon nanotubes for Li-ion batteries, *Electrochimica Acta* **2006**, *51*, 4994-5000.
(9) Y. Chen, M. Nie, B. L. Lucht, A. Saha, P. R. Guduru, A. Bose High Capacity, Stable Silicon/Carbon Anodes for Lithium-Ion Batteries Prepared Using Emulsion-Templated Directed Assembly, *ACS Applied Materials & Interfaces* **2014**, *6*, 4678-4683.
(10) S. Jeong, E. C. Garnett, S. Wang, Z. Yu, S. Fan, M. L. Brongersma, M. D. McGehee, Y. Cui Hybrid Silicon Nanocone–Polymer Solar Cells, *Nano Letters* **2012**, *12*, 2971-2976.
(11) J. Yeom, D. Ratchford, C. R. Field, T. H. Brintlinger, P. E. Pehrsson Decoupling Diameter and Pitch in Silicon Nanowire Arrays Made by Metal-Assisted Chemical Etching, *Advanced Functional Materials* **2014**, *24*, 106-116.
(12) B. Karthik, S. S. Jyothi, S. Jae Cheol, A. Bruno, C. Debashis, M. Mohammad, H. Keng, A. R. John, F. Placid, S. Sanjiv, L. Xiuling Porosity control in metal-assisted chemical etching of degenerately doped silicon nanowires, *Nanotechnology* **2012**, *23*, 305304.
(13) Z. Shenli, W. Xinwei, L. Hong, S. Wenzhong Controllable light-induced conic structures in silicon nanowire arrays by metal-assisted chemical etching, *Nanotechnology* **2014**, *25*, 025602.
(14) Y. Hu, K.-Q. Peng, L. Liu, Z. Qiao, X. Huang, X.-L. Wu, X.-M. Meng, S.-T. Lee Continuous-flow Mass Production of Silicon Nanowires via Substrate-Enhanced Metal-Catalyzed Electroless Etching of Silicon with Dissolved Oxygen as an Oxidant, *Sci. Rep.* **2014**, *4*.
(15) J.-S. Wi, H.-S. Lee, K. Lim, S.-W. Nam, H.-M. Kim, S.-Y. Park, J. J. Lee, C. D. Hong, S. Jin, K.-B. Kim Fabrication of Silicon Nanopillar Teradot Arrays by Electron-Beam Patterning for Nanoimprint Molds, *Small* **2008**, *4*, 2118-2122.
(16) G. Alexandre, B. Jean, T. Bernard Creating nanostructures on silicon using ion blistering and electron beam lithography, *Nanotechnology* **2006**, *17*, 600.
(17) R. Juhasz, J. Linnros Silicon nanofabrication by electron beam lithography and laser-assisted electrochemical size-reduction, *Microelectronic Engineering* **2002**, *61–62*, 563-568.
(18) T. Gorisse, L. Dupré, P. Gentile, M. Martin, M. Zelsmann, D. Buttard Highly organised and dense vertical silicon nanowire arrays grown in porous alumina template on <100> silicon wafers, *Nanoscale Research Letters* **2013**, *8*, 287-287.
(19) H. Sugimura, N. Nakagiri Fabrication of silicon nanostructures through scanning probe anodization followed by chemical etching, *Nanotechnology* **1995**, *6*, 29.
(20) D. Neiner, S. M. Kauzlarich Hydrogen-Capped Silicon Nanoparticles as a Potential Hydrogen Storage Material: Synthesis, Characterization, and Hydrogen Release, *Chemistry of Materials* **2010**, *22*, 487-493.
(21) J. R. Heath A Liquid-Solution-Phase Synthesis of Crystalline Silicon, *Science* **1992**, *258*, 1131-1133.
(22) X. Lu, B. A. Korgel A Single-Step Reaction for Silicon and Germanium Nanorods, *Chemistry – A European Journal* **2014**, *20*, 5874-5879.
(23) T. D. Bogart, X. Lu, B. A. Korgel Precision synthesis of silicon nanowires with crystalline core and amorphous shell, *Dalton Transactions* **2013**, *42*, 12675-12680.
(24) S. K. Cho, F. R. F. Fan, A. J. Bard Formation of a silicon layer by electroreduction of SiO 2 nanoparticles in CaCl 2 molten salt, *Electrochimica Acta* **2012**, *65*, 57-63.
(25) L. Y. A. Markovski Chemistry of Magnesiothermal Preparation of Boron, *Electron Technol* **1970**, *3*, 95-102.
(26) V. F. Baibuz, V. Y. Zitserman, S. I. Gorbov, Y. N. Olkhov, V. V. Golikov THERMODYNAMICS OF THE MAGNESIOTHERMIC REDUCTION OF TITANIUM TETRACHLORIDE, *Russian metallurgy. Metally* **1986**, 43-47.
(27) A. A. Zakharevich, R. A. Sandler, S. V. Aleksandrovskii Modeling OF Recrystallization Processes in Magnesiothermic Production of Sponge Titanium, *Journal of applied chemistry of the USSR* **1987**, *60*, 78-81.
(28) Z. Bao, M. R. Weatherspoon, S. Shian, Y. Cai, P. D. Graham, S. M. Allan, G. Ahmad, M. B. Dickerson, B. C. Church, Z. Kang, H. W. Abernathy Iii, C. J. Summers, M. Liu, K. H. Sandhage Chemical reduction of three-dimensional silica micro-assemblies into microporous silicon replicas, *Nature* **2007**, *446*, 172-175.
(29) K. H. Kim, D. J. Lee, K. M. Cho, S. J. Kim, J.-K. Park, H.-T. Jung Complete magnesiothermic reduction reaction of vertically aligned mesoporous silica channels to form pure silicon nanoparticles, *Sci. Rep.* **2015**, *5*.
(30) M. Nagamori, I. Malinsky, A. Claveau Thermodynamics of the Si-C-O system for the production of silicon carbide and metallic silicon, *MTB* **1986**, *17*, 503-514.
(31) W. Luo, X. Wang, C. Meyers, N. Wannenmacher, W. Sirisaksoontorn, M. M. Lerner, X. Ji Efficient Fabrication of Nanoporous Si and Si/Ge Enabled by a Heat Scavenger in Magnesiothermic Reactions, *Sci. Rep.* **2013**, *3*.
(32) J. Zhu, J. Wu, Y. Wang, C. Meng Synthesis and characterization of mesoporous silicon directly from pure silica sodalite single crystal, *J Mater Sci* **2010**, *45*, 6769-6774.
(33) J. Xie, G. Wang, Y. Huo, S. Zhang, G. Cao, X. Zhao Hollow nano silicon prepared by a controlled template direction and magnesiothermic reduction reaction as anode for lithium ion batteries, *New Journal of Chemistry* **2014**, *38*, 4177-4181.
(34) W. Wang, J. C. Martin, R. Huang, W. Huang, A. Liu, A. Han, L. Sun Synthesis of silicon complexes from rice

husk derived silica nanoparticles, *RSC Advances* **2012**, *2*, 9036-9041.
(35) N.-M. D. Courchesne, M. T. Klug, P.-Y. Chen, S. E. Kooi, D. S. Yun, N. Hong, N. X. Fang, A. M. Belcher, P. T. Hammond Assembly of a Bacteriophage-Based Template for the Organization of Materials into Nanoporous Networks, *Advanced Materials* **2014**, *26*, 3398-3404.
(36) P.-Y. Chen, M. N. Hyder, D. Mackanic, N.-M. D. Courchesne, J. Qi, M. T. Klug, A. M. Belcher, P. T. Hammond Assembly of Viral Hydrogels for Three-Dimensional Conducting Nanocomposites, *Advanced Materials* **2014**, *26*, 5101-5107.
(37) M. Sumper, N. Kroger Silica formation in diatoms: the function of long-chain polyamines and silaffins, *Journal of Materials Chemistry* **2004**, *14*, 2059-2065.
(38) J. N. Cha, K. Shimizu, Y. Zhou, S. C. Christiansen, B. F. Chmelka, G. D. Stucky, D. E. Morse Silicatein filaments and subunits from a marine sponge direct the polymerization of silica and silicones in vitro, *Proceedings of the National Academy of Sciences* **1999**, *96*, 361-365.
(39) A. Rai, C. C. Perry Facile Fabrication of Uniform Silica Films with Tunable Physical Properties Using Silicatein Protein from Sponges, *Langmuir* **2010**, *26*, 4152-4159.
(40) R. L. Brutchey, D. E. Morse Silicatein and the Translation of its Molecular Mechanism of Biosilicification into Low Temperature Nanomaterial Synthesis, *Chemical Reviews* **2008**, *108*, 4915-4934.
(41) C. Mao, D. J. Solis, B. D. Reiss, S. T. Kottmann, R. Y. Sweeney, A. Hayhurst, G. Georgiou, B. Iverson, A. M. Belcher Virus-Based Toolkit for the Directed Synthesis of Magnetic and Semiconducting Nanowires, *Science* **2004**, *303*, 213-217.
(42) Y. D. Tu, Z. Zhou, R. J. Yan, Y. P. Gan, W. Z. Huang, X. X. Weng, H. Huang, W. K. Zhang, X. Y. Tao Bio-template synthesis of spirulina/TiO2 composite with enhanced photocatalytic performance, *RSC Advances* **2012**, *2*, 10585-10591.
(43) X. Zhang, M. Yu, J. Liu, S. Li Bioinspired Synthesis of a Hollow Metallic Microspiral Based on a Spirulina Bioscaffold, *Langmuir* **2012**, *28*, 3690-3694.
(44) K. Kamata, Z. Piao, S. Suzuki, T. Fujimori, W. Tajiri, K. Nagai, T. Iyoda, A. Yamada, T. Hayakawa, M. Ishiwara, S. Horaguchi, A. Belay, T. Tanaka, K. Takano, M. Hangyo Spirulina-Templated Metal Microcoils with Controlled Helical Structures for THz Electromagnetic Responses, *Sci. Rep.* **2014**, *4*.
(45) L. Shen, X. Guo, X. Fang, Z. Wang, L. Chen Magnesiothermically reduced diatomaceous earth as a porous silicon anode material for lithium ion batteries, *Journal of Power Sources* **2012**, *213*, 229-232.
(46) S. Chandrasekaran, M. J. Sweetman, K. Kant, W. Skinner, D. Losic, T. Nann, N. H. Voelcker Silicon diatom frustules as nanostructured photoelectrodes, *Chemical Communications* **2014**, *50*, 10441-10444.
(47) W.-T. Tsai, C.-W. Lai, K.-J. Hsien Characterization and adsorption properties of diatomaceous earth modified by hydrofluoric acid etching, *Journal of Colloid and Interface Science* **2006**, *297*, 749-754.
(48) M. Guo, X. Zou, H. Ren, F. Muhammad, C. Huang, S. Qiu, G. Zhu Fabrication of high surface area mesoporous silicon via magnesiothermic reduction for drug delivery, *Microporous and Mesoporous Materials* **2011**, *142*, 194-201.
(49) T.-D. Nguyen, J. A. Kelly, W. Y. Hamad, M. J. MacLachlan Magnesiothermic Reduction of Thin Films: Towards Semiconducting Chiral Nematic Mesoporous Silicon Carbide and Silicon Structures, *Advanced Functional Materials* **2015**, *25*, 2175-2181.
(50) M. Raposo, R. de Morais, A. Bernardo de Morais Bioactivity and Applications of Sulphated Polysaccharides from Marine Microalgae, *Marine Drugs* **2013**, *11*, 233-252.
(51) D. Oh, X. Dang, H. Yi, M. A. Allen, K. Xu, Y. J. Lee, A. M. Belcher Graphene sheets stabilized on genetically engineered M13 viral templates as conducting frameworks for hybrid energy storage materials, *Small (Weinheim an der Bergstrasse, Germany)* **2012**, *8*, 1006-1011.
(52) H. Sigmund, D. Weiß, in *Ion Implantation: Equipment and Techniques, Vol. 11* (Eds.: H. Ryssel, H. Glawischnig), Springer Berlin Heidelberg, **1983**, pp. 473-480.
(53) E. Meng, *Biomedical Microsystems*, Taylor & Francis, **2011**.
(54) C. Rosant, B. Avalle, D. Larcher, L. Dupont, A. Friboulet, J.-M. Tarascon Biosynthesis of Co3O4 electrode materials by peptide and phage engineering: comprehension and future, *Energy & Environmental Science* **2012**, *5*, 9936-9943.
(55) A. S. Khalil, J. M. Ferrer, R. R. Brau, S. T. Kottmann, C. J. Noren, M. J. Lang, A. M. Belcher Single M13 bacteriophage tethering and stretching, *Proceedings of the National Academy of Sciences* **2007**, *104*, 4892-4897.
(56) J.-H. Eom, Y.-W. Kim, S. Raju Processing and properties of macroporous silicon carbide ceramics: A review, *Journal of Asian Ceramic Societies* **2013**, *1*, 220-242.
(57) M. Fukushima, Y. Zhou, Y.-I. Yoshizawa Fabrication and microstructural characterization of porous silicon carbide with nano-sized powders, *Materials Science and Engineering: B* **2008**, *148*, 211-214.
(58) J. Shi, F. Xu, P. Zhou, J. Yang, Z. Yang, D. Chen, Y. Yin, D. Chen, Z. Ma Refined nano-textured surface coupled with SiNx layer on the improved photovoltaic properties of multi-crystalline silicon solar cells, *Solid-State Electronics* **2013**, *85*, 23-27.
(59) C. Gladden, M. Gharghi, T. Zentgraf, Y. Liu, X. Yin, J. Valentine, X. Zhang, in *Optics InfoBase Conference Papers*, **2011**.
(60) X. Li, L. Zhang, X. Yin, Z. Yu Mechanical and dielectric properties of porous Si3N4–SiC(BN) ceramic, *Journal of Alloys and Compounds* **2010**, *490*, L40-L43.

Table of Content Graphic

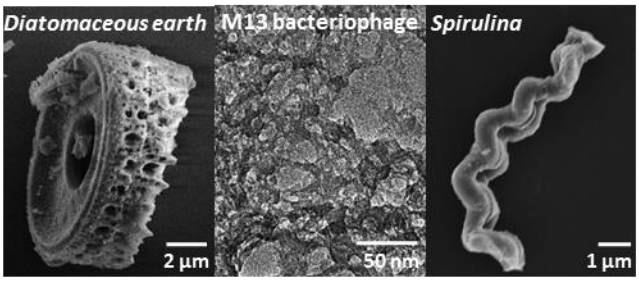

Supporting Information

Biotemplated Silica and Silicon Materials as Building Blocks for Micro- to Nanostructures

Noémie-Manuelle Dorval Courchesne,[⊥§] Stephen A. Steiner III,[‡§] Victor J. Cantú,[‡§] Paula T. Hammond,*[⊥§] Angela M. Belcher*[‡§]

Process Optimization

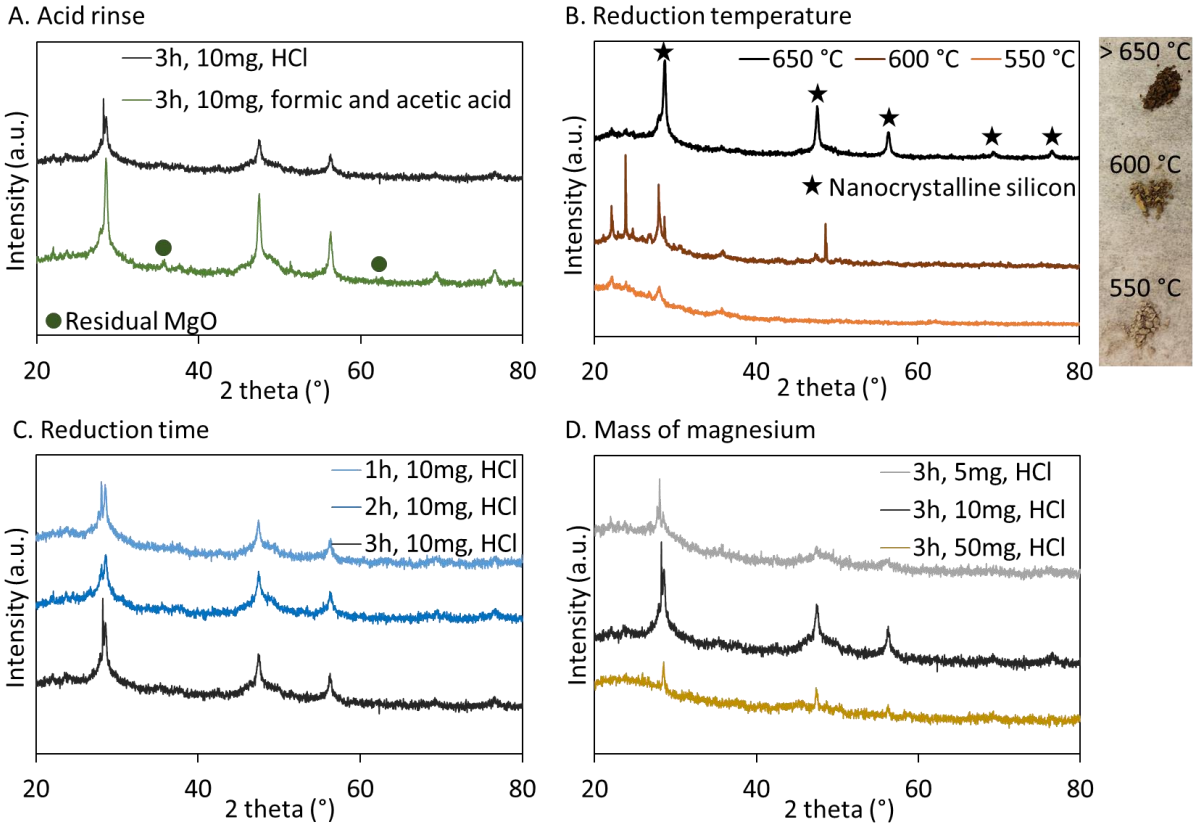

Figure S1. Magnesiothermal reduction is optimized with diatomaceous earth as a model organism, varying A. the acid used to rinse the product, B. the reduction temperature, C. reduction time at 650 °C, and D. the mass of magnesium for a 10 mg silica sample at 650 °C. Conversion of amorphous silica to nanocrystalline silicon indicates a successful reaction, and complete removal of MgO yields a clean product.

The acid rinse step used to purify the final silicon products was studied in detail. First, the disappearance of any remaining magnesium oxide was confirmed via XPS, and corroborates the XRD spectrum after HCl rinse presented in Figure S1. XPS also confirmed that the silicon product is covered with MgO before acid etch, and that after etching, the metalloid silicon chemistry is still visible in addition to surface oxides. Figure S2A shows the complete

disappearance of MgO from biotemplated silicon samples and the detection of silicon before and after magnesiothermal reduction of silicon templated onto layer-by-layer assembled bacteriophage thin films. The peak observed around 50.2 eV, indicative of the presence of MgO after magnesiothermal reduction, disappears upon rinsing with HCl. In addition, Figure S2B shows that, before acid etching, the silicon signal was weak, but it becomes apparent that the sample contains bulk metalloid silicon after rinsing with acid and uncovering the silicon surface.

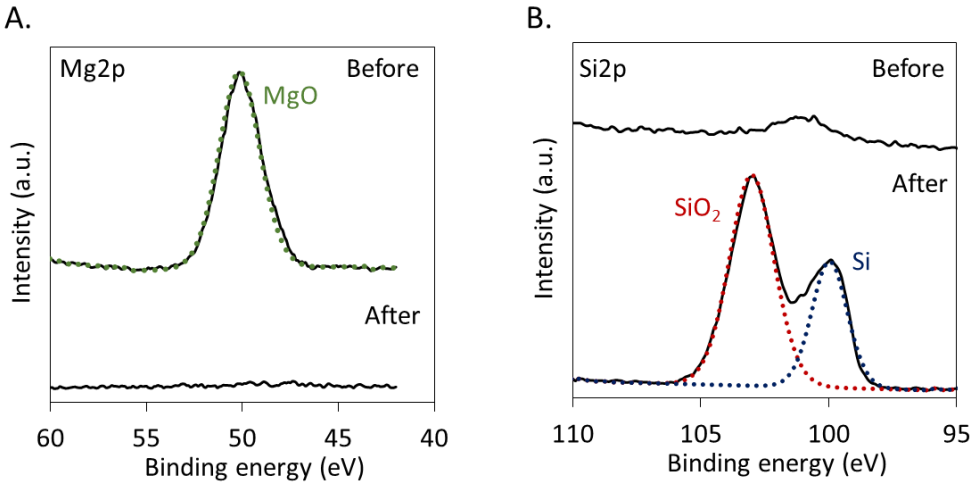

Figure S2. After rinsing with hydrochloric acid, magnesium oxide is completely cleaned off of the silicon product, uncovering the surface of reduced biotemplated silicon. XPS spectra of the A. Mg2p and B. Si2p regions for silicon templated onto LbL assembled M13 bacteriophage thin films, before and after rinsing with acid. Solid lines indicate the raw data, and dotted lines show fitted data, using Casa XPS.

Morphology of Biotemplated Silicon

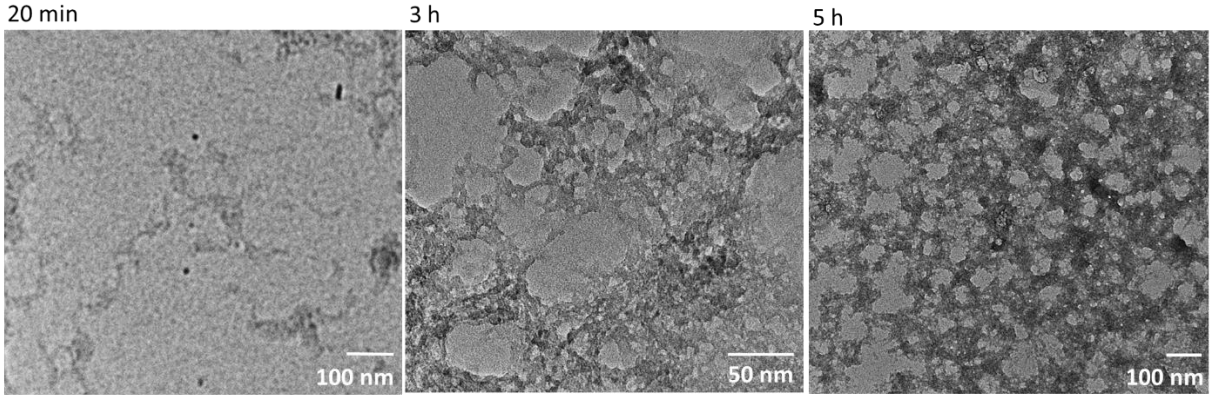

Figure S3. M13 bacteriophage-templated silica nanowire's morphology changes drastically with TMOS hydrolysis time. TEM images of the reaction product after 30 min, 3 h and 5 h.

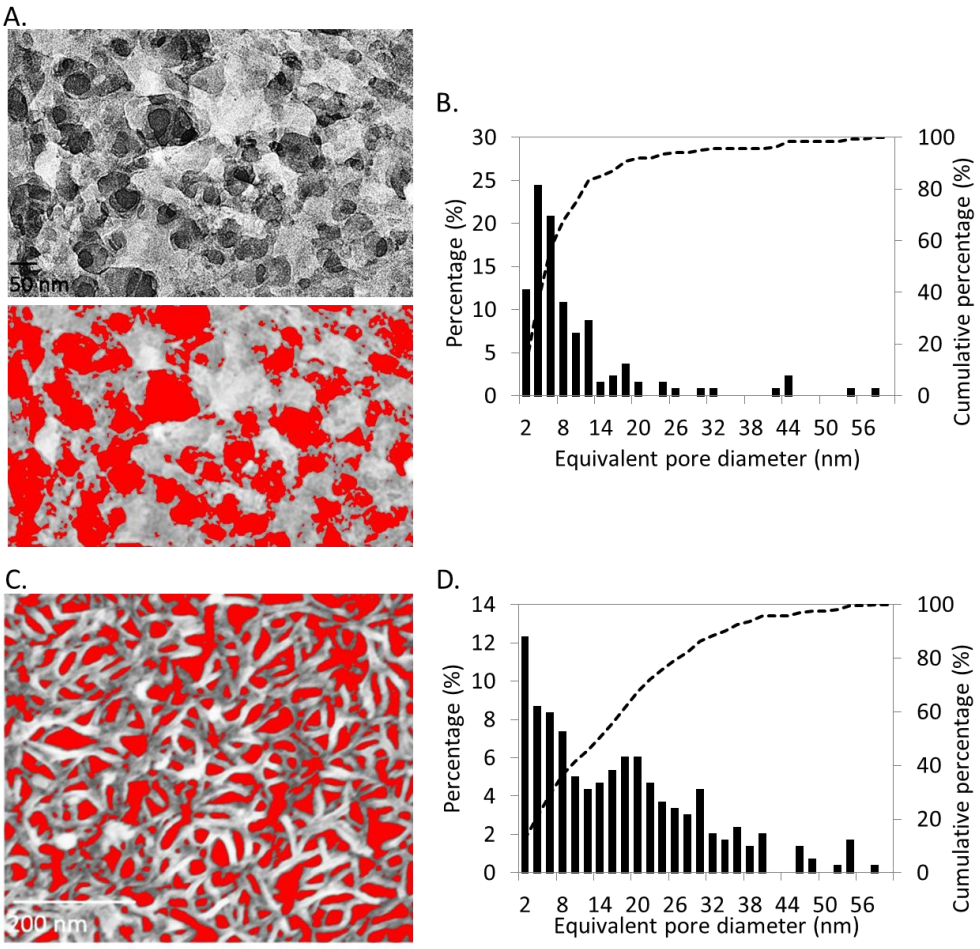

Figure S4. Bacteriophage-templated silicon structures are highly porous. A. TEM image of silicon templated from bacteriophages in solution (The contrast of the image was enhanced, and the colors were inverted (top panel). The pores were then identified using a color threshold,

shown in red (bottom panel).), and B. corresponding pore size distribution. C. SEM image of a bacteriophage-templated silicon thin film with pores identified in red, and D. corresponding pore size distribution. In B and D, bar graphs represent the percentage of pores for each equivalent pore diameter, and dashed lines correspond to the cumulative percentages. All analyses were performed using the ImageJ software.

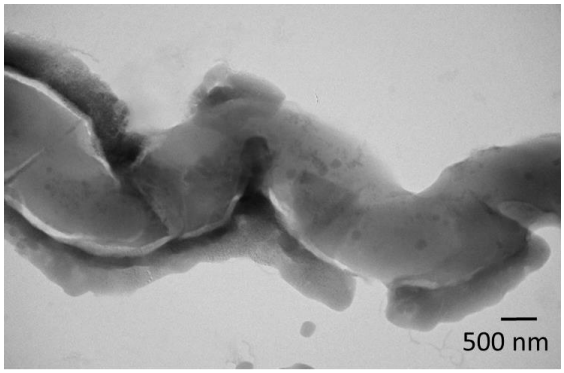

Figure S5. TEM image of *Spirulina major* with its polysaccharide outer layer.

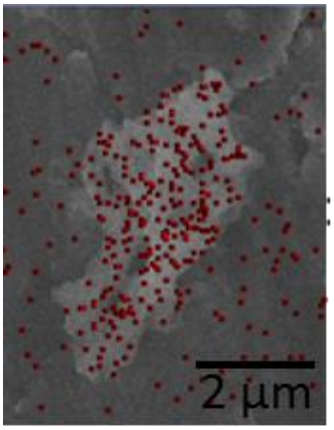

Figure S6. SEM image with elemental mapping of silicon for *Spirulina*-templated silicon deposited on titanium foil as substrate. Red squares indicate the mapping on silicon atoms.

BET Surface Area Analysis

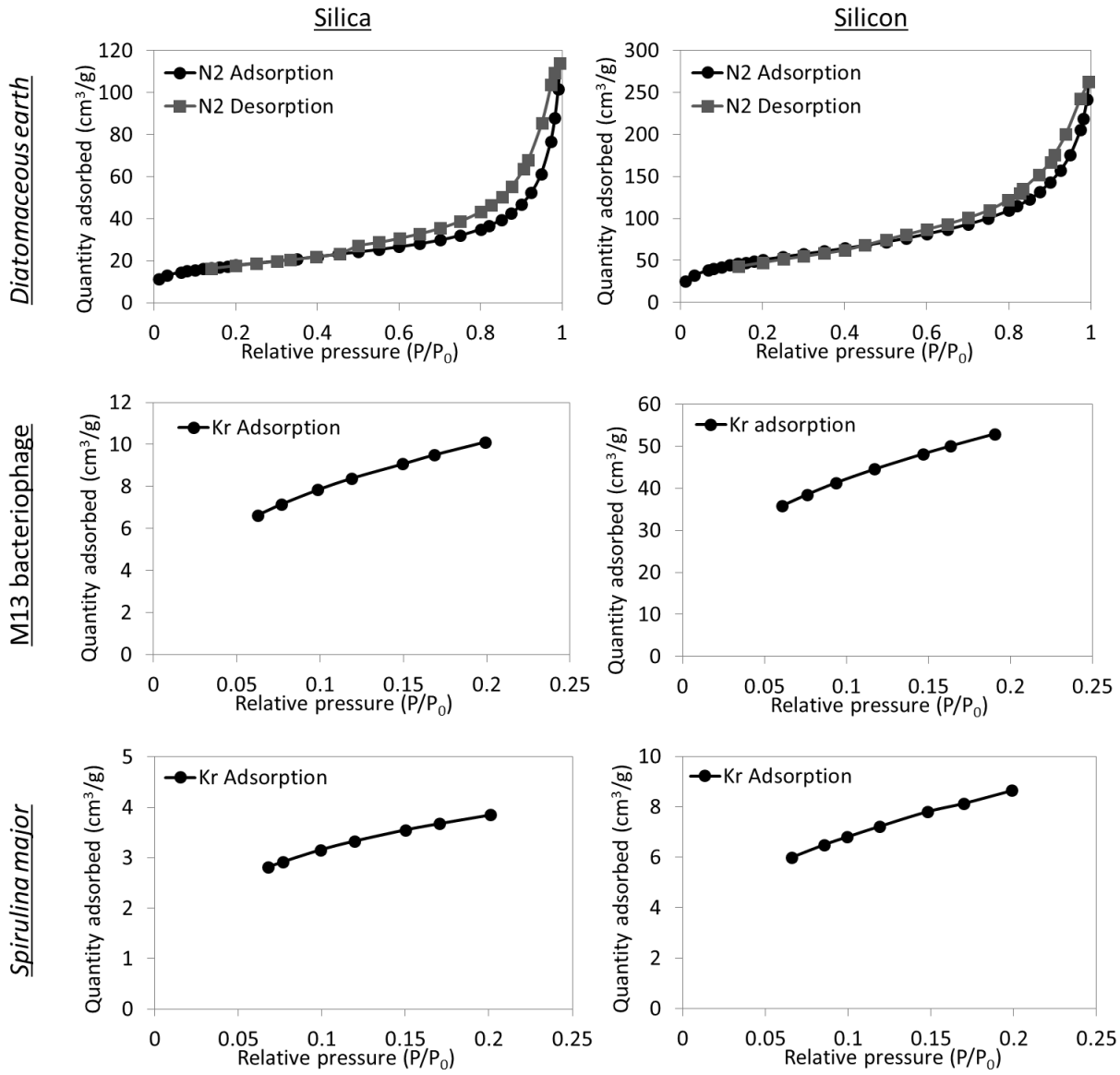

Figure S7. Biotemplated silica and silicon materials exhibit a higher surface area after magnesiothermal reduction. BET adsorption and desorption isotherms for the data presented in Table 1 are shown. For a small amount of material, krypton was used as the adsorbing gas to replace nitrogen.

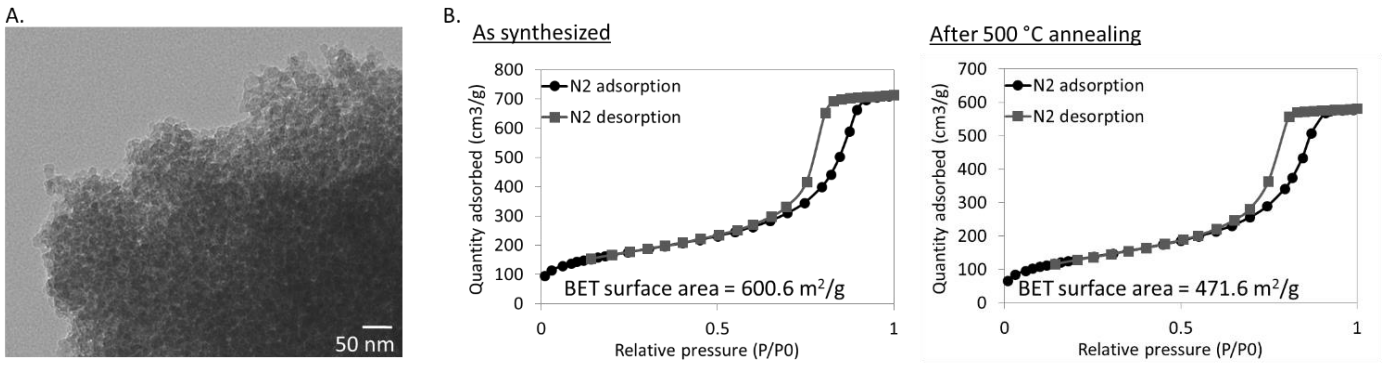

Figure S8. Silica nanoparticle control reaction produces a nanoparticle gel with randomly-organized nanoparticles, with a high surface area. A. Morphology of silica nanoparticles synthesized via TMOS hydrolysis without biotemplate. B. BET nitrogen adsorption and desorption isotherms for silica nanoparticles as synthesized, and silica nanoparticles exposed to a 500 °C heat treatment. The corresponding BET surface area is indicated. For silica nanoparticles as synthesized, the surface area reaches 600 m^2/g, and it decreases to 471 m^2/g after annealing. Compared to biotemplated silica samples (after annealing), the surface area of spherical nanoparticles is considerably larger.

Sodium Removal via Water Rinses

High sodium concentrations in bacteriophage-templated silicon before rinsing are due to the highly concentrated polyethylene glycol/sodium chloride solutions used to precipitate the bacteriophages during purification steps prior to biomineralization**.** Figure S9 shows the differences in sodium to silicon atomic ratio when rinse steps are added after drying the silica-mineralized bacteriophages, or after annealing the product to burn off the template. As more rinse steps are performed the content of Na decreases and can be reduced to practically zero. Therefore, although large amounts of Na are initially present in the phage-templated structures, rinses allow us to control final Na concentration.

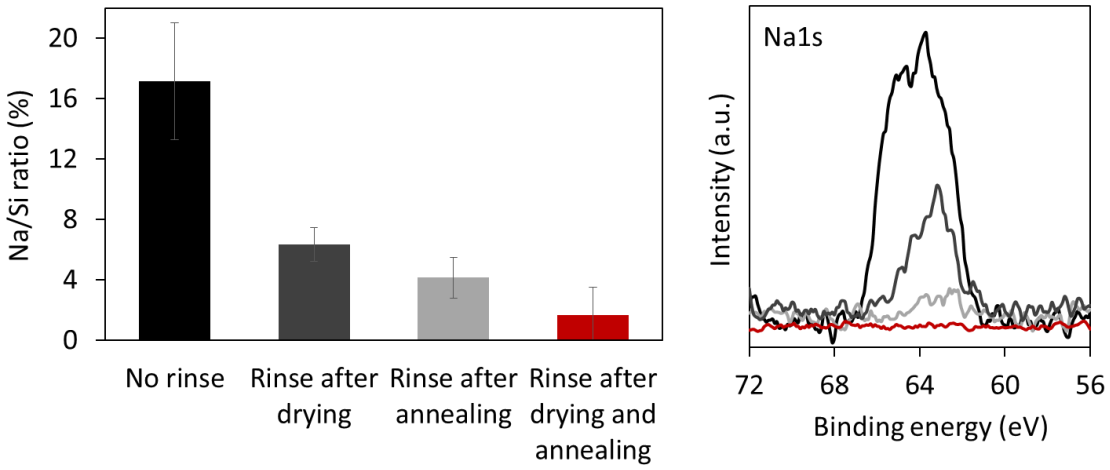

Figure S9. Water rinses allow for controlling the sodium content in the final M13 bacteriophage-templated silicon nanonetworks. Na to Si atomic ratio under different rinse conditions (left), and Na1s XPS spectrum for the corresponding conditions (right).

Synthesis of Silicon Carbide and Nitride

Figure S10 shows a XPS analysis for LbL-assembled M13 bacteriophage film coated with silica, and subsequently magnesiothermally reduced under nitrogen, without burning off the bacteriophage scaffold. As expected, both silicon nitride (Si2p peak around 101.8 eV) and silicon carbide (Si2p peak around 100.2 eV) are found in the final product, in addition to silica. Significant quantities of carbon and nitrogen were detected in the final product, with a ratio of Si:C of approximately 1:2, and Si:N of 12:1 on the surface based on a survey scan. Please note that carbon contaminants on the surface might have increased artificially the Si:C ratio. Based on the area of the fitted peaks in the Si2p spectrum after magnesiothermal reduction, the ratios of nitride:carbide:oxide formed was estimated to 1:2.3:2.7.

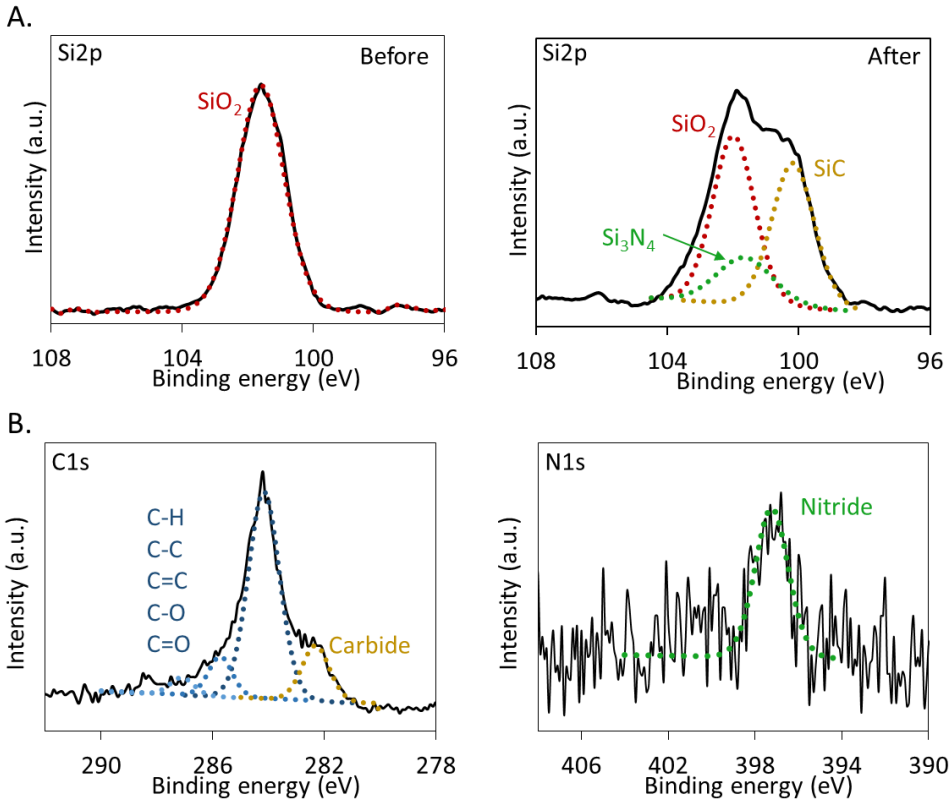

Figure S10. Magnesiothermal reduction of biotemplate silica under nitrogen and without burning off the biotemplate results in the synthesis of silicon carbide and silicon nitride. XPS spectra of A. the Si2p region before reduction, after MGTR and after acid rinse, and B. the N1s, and C1s regions for the final product after MGTR and acid rinse. The biotemplate used here was a LbL assembled M13 bacteriophage thin film.